Desalination and Water Treatment
www.deswater.com
doi: 10.5004/dwt.2018.22080

106 (2018) 200–208
February

Preparation of ZIF-8 nanoparticle-decorated Zn_2GeO_4 nanorods with high photocatalytic performance for chromium (VI) reduction

Shumin Wu[a], Yan Xu[a,*], Min Liu[a], Xianliang Li[b], Xia Zhang[a]

[a]*Department of Chemistry, College of Science, Northeastern University, Shenyang, Liaoning 110819, China, email: 1142136672@qq.com (S. Wu), Tel. +86-024-83684533, Fax +86-024-83684533, email: xuyanjlu@126.com (Y. Xu), liumin06180301@126.com (M. Liu), xzhang@mail.neu.edu.cn (X. Zhang)*
[b]*College of Materials Science and Engineering, Shenyang University of Chemical Technology, Shenyang, Liaoning 110142, China, email: lixianliang007@163.com (X. Li)*

Received 19 September 2017; Accepted 19 February 2018

ABSTRACT

Zeolitic imidazolate framework-8 (ZIF-8) nanoparticles decorated Zn_2GeO_4 composites, denoted as ZIF-8@Zn_2GeO_4, were prepared through a chemical deposition route. The obtained ZIF-8@Zn_2GeO_4 heterostructure was characterized by X-ray diffraction, scanning electron microscopy, infrared spectroscopy, and UV-Vis diffuse reflectance spectroscopy. The results showed that the ZIF-8 nanoparticles have been successfully assembled on the surface of Zn_2GeO_4 nanorods, and 100 mg of ZIF-8@Zn_2GeO_4 photocatalyst can reduce nearly 100% of Cr(VI) in aqueous solution (100 mL 1 × 10^{-5} mol L^{-1}) in 90 min under UV-light irradiation. The obtained ZIF-8@Zn_2GeO_4 photocatalysts exhibited 14.1 and 1.8 times higher photocatalytic activity toward the photoreduction of Cr(VI) than pure Zn_2GeO_4 nanorods and ZIF-8 under UV light irradiation, respectively. The synthetic strategy used is also promising for implementing MOF structures in other semiconductor photocatalysts for reduction of Cr(VI) to Cr(III) with enhanced photocatalytic performance and high stability in aqueous media.

Keywords: Photocatalysts; Zn_2GeO_4; Metal-organic framework; Cr(VI); Light irradiation

1. Introduction

Cr(VI) is a highly toxic and dangerous contaminant in industrial wastewater that needs to be treated before being released. Generally, it is highly mobile in water and exhibits a high toxicity and carcinogenicity for human beings [1,2]. Therefore, reducing the concentration of Cr(VI) in wastewater has aroused widespread concerns [3–8]. Many conventional methods such as ion exchange, membrane separation, adsorption, chemical precipitation and photocatalysis have been used for the treatment of Cr(VI) in wastewater. Among them, photocatalysis has been proven to be a useful approach in reducing Cr(VI) to Cr(III) and the precipitation of the latter from water under neutral or alkaline condition [9]. Up to now, a large number of photocatalysts based on semiconductors such as TiO_2 [10–16], SnO_2 [17], Co_3O_4 [18], WO_3 [19,20], ZnO [21–26], $ZnFe_2O_4$ [27], and Zn_2GeO_4 [28] have been reported.

Zn_2GeO_4, as a ternary metal oxide with wide band gap of 4.68 eV, has been widely investigated as a photocatalyst due to its stable and efficient photocatalytic activity. However, the Cr(VI) ions are usually difficult to achieve to the active sites on the surface of Zn_2GeO_4 photocatalyst, which restricts its practical application for the photoreduction of Cr(VI). Thus, increasing the Cr(VI) reactive sites on the surface of Zn_2GeO_4 photocatalysts is an effective way in improving its photocatalytic activity.

Metal organic frameworks (MOFs), a new class of crystalline porous materials, have been proven to be a promising candidate material for photocatalytic reaction, for examples, water splitting, CO_2 reduction, and photodegradation of organic pollutant [29]. However, the MOF photocatalysts usually show low efficiency in exciton generation and charge separation in comparing

*Corresponding author.

with the traditional semiconductor photocatalysts, which greatly restrict its practical application. Thus, integrating the superiority of reactant adsorption performance of MOF together with the high photocatalytic performance of semiconductor can provide a promising strategy in exploring new photocatalysts. For instance, Wang and coworkers firstly synthesized a ZIF-8 nanoparticle functionalized Zn_2GeO_4 hybrid photocatalyst, and they found that the composite exhibited higher photocatalytic activity for CO_2 photoreduction than the bare Zn_2GeO_4 in the aqueous system [30]. Aside from this example, many other MOF@semiconductor composites [31–34], such as C_3N_4/Co-ZIF-9 [31], TiO_2@ZIF-8 [32], ZnO@ZIF-8 [33] and CPO-27-Mg/TiO_2 [34] have been reported and used as photocatalysts in various applications. Overall, these previous works have well illustrated that the combination of MOF and semiconductor has higher photocatalytic activity than the single component due to their synergistic effect.

In this paper, a similar MOF@semiconductor hybrid structure of ZIF-8@Zn_2GeO_4, was prepared by decorating the surface of Zn_2GeO_4 semiconductor with nanosized ZIF-8 particles via a simpler modified chemical deposition route. ZIF-8 was chosen as MOF material due to its excellent thermal and chemical stability [35]. Compared to pure Zn_2GeO_4 semiconductor, the ZIF-8@Zn_2GeO_4 exhibits significantly enhanced photocatalytic activity in reducing Cr(VI) to Cr(III) under 300 W Xe lamp (λ = 300–700 nm) irradiation at room temperature, which was benefiting from the strong Cr(VI) adsorption on the surface of ZIF-8, as well as the more efficient charge transfer process between ZIF-8 and Zn_2GeO_4 semiconductor.

2. Experimental

2.1. Materials

All of the reagents are analytical grade regents and used as received without further purification. GeO_2 (germanium dioxide, 99.99%, China), Zinc Acetate ($Zn(CH_3COO)_2{\cdot}2H_2O$, 98% Fuchen, Tianjin, China), sodium hydroxide (NaOH, 99.5%, Guoyao, Shanghai, China), methanol (99.7%, Yongda, Tianjin, China), 2-methylimidazole (99%, Sigma-Aldrich), and pure water (Wahaha, purified drinking water, China). Stock solution of Cr(VI) was prepared by dissolving the analytical grade $K_2Cr_2O_7$ (99%, Yongda, Tianjin, China) powder in pure water.

2.2. Preparation of Zn_2GeO_4 and ZIF-8@ Zn_2GeO_4

The Zn_2GeO_4 nanorods were prepared by one-pot hydrothermal method using sodium hydroxide instead of 25% tetramethylammonium hydroxide (TMAOH) aqueous solution according to the synthetic method reported in Ref. [30]. Briefly, 1.04 g of GeO_2 (10.0 mmol) and 2.195 g of $Zn(CH_3COO)_2{\cdot}2H_2O$ (10.0 mmol) were dissolved into pure water (60 mL) under continuous stirring for 30 min. The pH value of the solution was adjusted to 8 by the addition of 0.1 mol L^{-1} sodium hydroxide solution. The mixture was then transferred and sealed in a 100 mL Teflon-lined autoclave and heated at 140°C for 24 h in a convection oven, followed by cooling naturally to room temperature. The white Zn_2GeO_4 powder was collected by centrifugation, washed thoroughly with pure water and ethanol for several times, and then dried at 60°C for 12 h.

About 0.4 g of as-prepared Zn_2GeO_4 nanorods and 0.587 g of $Zn(NO_3)_2{\cdot}6H_2O$ were added to MeOH (40 mL) of and stirred for 1 h. A second solution was prepared by dissolving 1.298 g of 2-methylimidazole in MeOH (40 mL). The latter clear solution was poured into the former solution under magnetic stirring for another 1 h. The white ZIF-8@ Zn_2GeO_4 precipitate was collected and washed with distilled water and ethanol two times and dried at 60°C for 12 h.

2.3. Characterization

The phase of the as-prepared samples was characterized by powder X-ray diffraction on a X'Pert Pro MRDDY2094 diffractometer with Cu-Kα radiation (λ = 1.5418 Å). A scan rate of 0.0167 s^{-1} was used to record the XRD pattern in the 2*q* range of 6–70°. The morphologies of Zn_2GeO_4 nanorods and ZIF-8@Zn_2GeO_4 hybrids were observed using the Ultra Plus field-emission scanning electron microscope (SEM). The UV-visible adsorption spectra were recorded using a Hitachi U-3010 UV-visible spectrometer. FTIR spectra were recorded in the range of 4000–400 cm^{-1} on an Alpha Centaur FTIR spectrophotometer using KBr pellets. TEM was carried out on a Tecnai $G^2$20, and the TEM samples were ultrasonically dispersed in ethanol for 10 min followed by dropping a small amount of the solution on a holey carbon-coated copper grid and drying. Thermogravimetric analyses (TG) were performed using a Mettler Toledo TGA2 (LF) in air atmosphere with a heating rate of 10°C min^{-1}.

2.4. Photoelectrochemical measurement

Photocurrent measurements were performed on an electrochemical work station (Chenhua Instrument, Shanghai, China) in a standard three-electrode system with the photocatalyst-coated indium tin oxide (ITO) as the working electrode, Pt plate as the counter electrode, and an Ag/AgCl as a reference electrode. 0.2 M Na_2SO_4 was used as the electrolyte. About 4 mg of as-prepared sample was mixed with ethanol (0.2 mL), water (0.8 mL), and Nafion solution (20 μL), and the working electrode was prepared by dropping the suspension (80 μL) onto the surface of a 1 × 1 cm ITO plate. The working electrode was dried at room temperature, and the photoresponsive signals of the samples were measured under chopped light.

2.5. Photocatalytic test

The photocatalytic performance of the as-prepared ZIF-8@ Zn_2GeO_4 hybrids was evaluated by the degradation of Cr(VI) under a 300 W Xe lamp light irradiation (λ = 300–700 nm). Firstly, 0.10 g of ZIF-8@ Zn_2GeO_4 was dispersed in 100 mL 1 × 10^{-5} mol L^{-1} Cr(VI) solution. Prior to irradiation, the suspension was stirred in the dark for 30 min to ensure that the adsorption of Cr(VI) on the surface of catalyst had reached equilibrium. Then the reaction mixture was

irradiated in a photochemical reaction chamber with continuous stirring. 3 mL of supernate was taken out at a certain time of 30 min intervals and centrifuged to remove photocatalyst particles, to which 30 µL of H_2SO_4 (9.2 M) and 50 µL of 1,5-diphenylcarbazide (DPCI, 0.005 M, ethanol solution) were added to give a colored solution for Cr(VI) analysis. The concentration of Cr(VI) in the treated solution was measured by UV-vis spectroscopy.

3. Results and discussion

3.1. XRD analysis

XRD patterns of the as-prepared pure Zn_2GeO_4 nanorods and ZIF-8@Zn_2GeO_4 hybrids are shown in Fig. 1. All of the diffraction peaks of Zn_2GeO_4 nanorods are consistent with the simulated XRD pattern of the rhombohedral phase of Zn_2GeO_4 (JCPDS No. 11-0687) (Figs. 1a and 1b). There is no trace of impurity phase, such as ZnO and GeO_2. The simulated XRD pattern of ZIF-8 based on the reported crystal structure data (CCDC No. 602542) is shown in Fig. 1c. Compared with the pure Zn_2GeO_4 nanorods, the additional weak peaks appeared at 7.4°, 16.5°, 18.0° and 26.7° in the XRD pattern of ZIF-8@Zn_2GeO_4 hybrids (Fig. 1d) can be assigned to the characteristic peaks of ZIF-8 shell, suggesting that small amount of ZIF-8 composite has been successfully deposited on the surface of Zn_2GeO_4.

3.2. SEM and TEM analyses

The structure and morphology of the as-prepared Zn_2GeO_4 nanorods, and ZIF-8@ Zn_2GeO_4 hybrids were observed by SEM and TEM techniques. A large quantity of Zn_2GeO_4 nanorods with several micrometers in length and 50–100 nm in width can be seen in in Fig. 2a–d. Compared with the smooth surface of Zn_2GeO_4 nanorods shown in Fig. 2, it can be seen in Fig. 2e–h that the surfaces of Zn_2GeO_4 nanorods were successfully covered with a thin layer of ZIF-8. Meanwhile, the TEM images of ZIF-8@ Zn_2GeO_4 hybrids also demonstrated that the ZIF-8 nanoparticles had been successfully deposited on the external surface of Zn_2GeO_4 nanorods as is shown in Fig. 2i–l. The HRTEM image of the as-prepared ZIF-8@Zn_2GeO_4 hybrid with clear lattice fringes is shown in Fig. 3, and the lattice fringes with the spacing of 0.41 nm can be indexed to the (311) crystallographic planes of an orthorhombic Zn_2GeO_4. ZIF-8 is highly sensitive to the electron beam damage.

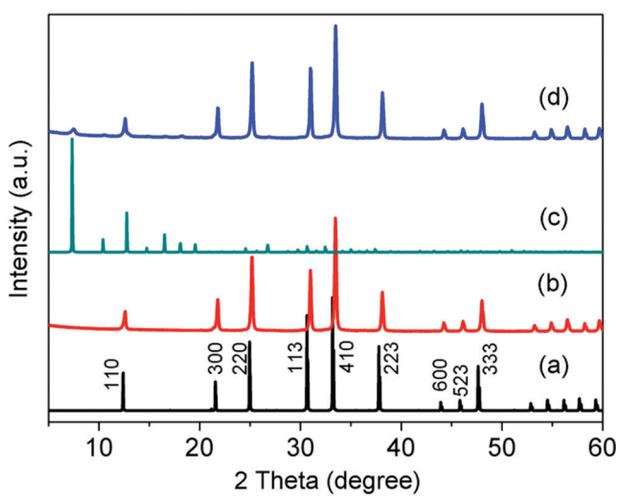

Fig. 1. Simulated powder XRD patterns of (a) Zn_2GeO_4, (b) as-prepared Zn_2GeO_4, (c) simulated XRD of ZIF-8, and (d) as-obtained ZIF-8@Zn_2GeO_4 hybrid.

3.3. IR, TG, and UV-Vis absorption spectra analyses

The chemical structures of the as-prepared Zn_2GeO_4 and ZIF-8@Zn_2GeO_4 hybrid were investigated by FTIR. As results are shown in Fig. 4a, the peaks appeared at 799 cm^{-1}, 749 cm^{-1}, and 535 cm^{-1} in ZIF-8@Zn_2GeO_4 hybrid can be assigned to the vibration modes of the ZnO_4 and GeO_4 tetrahedron. The peaks at 3135 cm^{-1} and 2929 cm^{-1} correspond to C–H stretches. The absorption peaks at 1305 cm^{-1}, 1145 cm^{-1}, and 759 cm^{-1} are associated with the bending signals of the imidazole ring [30], proving that the ZIF-8@ Zn_2GeO_4 hybrid composite has been successfully prepared. Thermogravimetric-differential thermal analysis (TG-DTA) was performed on a Mettler Toledo TGA2 (LF) to study the weight loss of organic species. The ZIF-8@Zn_2GeO_4 sample was heated from 25 to 900°C with a heating rate of 10°C/min in air, and the TG curves of ZIF-8@ Zn_2GeO_4 hybrid and Zn_2GeO_4 nanorods are shown in Fig. 4b–c. The weight loss of 7.02% between 25 and 550°C in the TG curve of ZIF-8@ Zn_2GeO_4 corresponds to the decomposition of 2-methylimidazole molecules in ZIF-8. Fig. 4d shows UV-vis absorption spectra of ZIF-8@ Zn_2GeO_4 hybrids and Zn_2GeO_4 nanorods. The absorption edge of ZIF-8@ Zn_2GeO_4 hybrids is extended slightly. According to the formula: $Eg = 1240/\lambda_g$, the band gap energy (Eg) of ZIF-8@Zn_2GeO_4 hybrids and Zn_2GeO_4 nanorods are estimated to be about 4.35 eV and 4.5 eV, respectively. However, the spectrum intensity of ZIF-8@Zn_2GeO_4 decreased obviously and was weaker than that of ZIF-8, which might be caused due to the excessive growth and aggregation of ZIF-8.

3.4. Raman spectroscopy and XPS measurements

The room temperature Raman spectrum of ZIF-8@ Zn_2GeO_4 is presented in Fig. 5a. The strongest peak centered at 801 cm^{-1} can be assigned to the stretching vibration of GeO_4 tetrahedral. The two peaks centered at 745, and 776 cm^{-1} were attributed to Ge-O-Zn symmetric and asymmetric vibrations, respectively [36]. The X-ray photoelectron spectroscopy (XPS) analysis confirms the presence of Zn, Ge, and O in both Zn_2GeO_4 and ZIF-8@Zn_2GeO_4 hybrid composites (Figs. 5b-d). The remarkable difference in the intensities of Zn, Ge, O peaks in each sample is an illustration of the different elemental concentrations.

3.5. Photoelectrochemical activity

In order to understand the energetic positions of the conduction band (V_{CB}) of ZIF-8@Zn_2GeO_4, Mott-Schottky

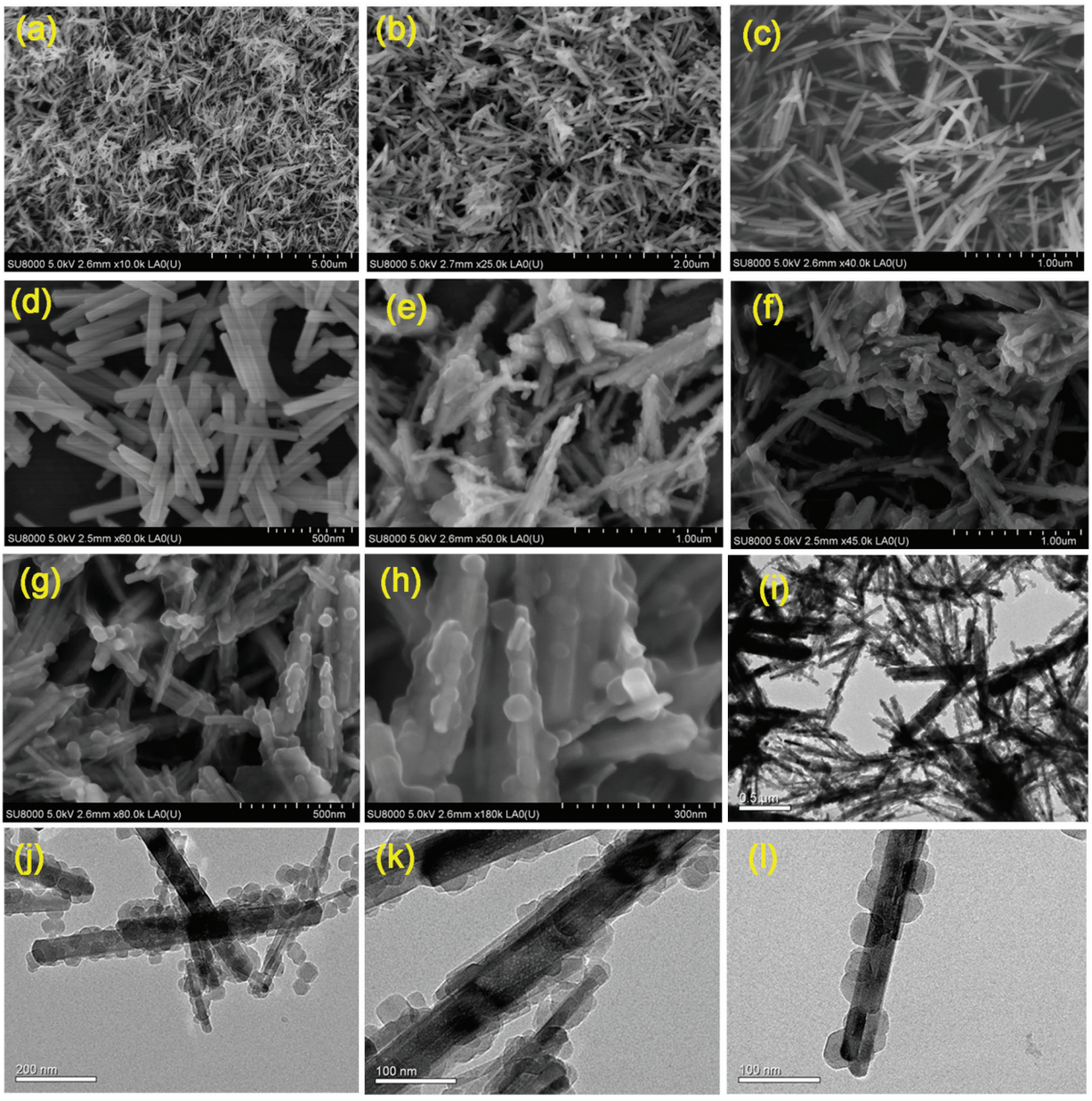

Fig. 2. (a–d) SEM images of as-prepared Zn_2GeO_4 nanorods and (e–h) ZIF-8@Zn_2GeO_4 hybrids; (i–l) TEM images of as-prepared ZIF-8@Zn_2GeO_4 hybrids.

Curves were measured [37]. The flat-band potential (E_{fb}) values can be obtained from the extrapolation of Mott-Schottky plots according to the following equation:

$$\frac{1}{C^2} = \frac{2}{ee_o N_D}\left(E - E_{fb} - \frac{k_b T}{q}\right)$$

where C is the space charge capacitance, e is the permittivity of free space, e_o is the permittivity of the semiconductor electrode, N_D is the donor density, E is the externally applied potential, E_{fb} is the flat-band potential at the semiconductor/electrolyte junction, k_b is Boltzmann's constant, T is the operation temperature, and q is the electronic charge. Fig. 6a shows the typical Mott-Schottky plots of the ZIF-8@Zn_2GeO_4 and Zn_2GeO_4. The positive slope of both Mott-Schottky plots indicated both samples are the n-type semiconductors. The flat-band potential of ZIF-8@Zn_2GeO_4 and Zn_2GeO_4 are approximately –0.9V (vs. Ag/AgCl) and –1.2V (vs. Ag/AgCl) at pH 7.0, respectively. The flat-band potential of the n-type semiconductor is particularly close to the bottom of the V_{CB}. Thus, the redox

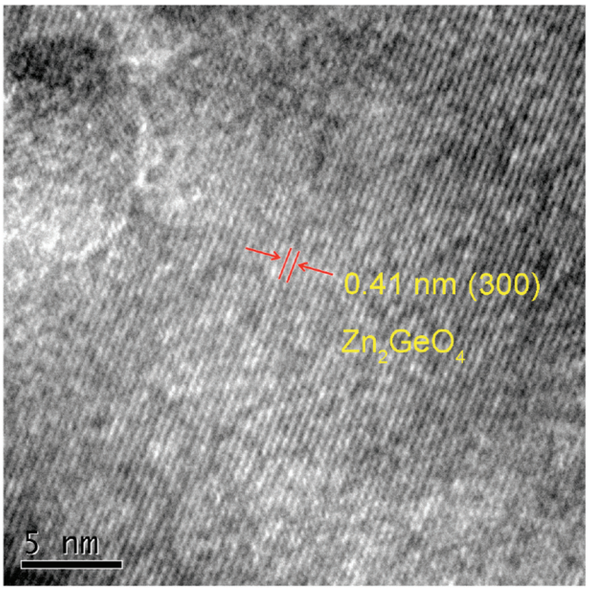

Fig. 3. HRTEM image of the as-prepared ZIF-8@Zn_2GeO_4 hybrid.

potential of conduction band (CB) of ZIF-8@Zn_2GeO_4 and Zn_2GeO_4 vs. Normal Hydrogen Electrode are –0.7 V and –1.0 V, respectively, which are more negative than Cr(VI)/Cr(III) potential (+0.51 V, pH 7.0). It is permissible for the transformation of photogenerated electrons to reduce Cr(VI) to Cr(III).

Photocurrent response has recently been applied to investigate the separation efficiency of photogenerated active carries for redox reactions. In general, the higher the photocurrent intensity, the better the separation efficiency of the photogenerated active carries [38]. Fig. 6b shows the photocurrent of ZIF-8, Zn_2GeO_4, and ZIF-8@ Zn_2GeO_4 samples under the irradiation of a 300 W Xe lamp in 0.2M Na_2SO_4 electrolyte solution. It can be seen that ZIF-8@ Zn_2GeO_4 hybrid exhibit stronger photocurrent response signals than that of ZIF-8 and Zn_2GeO_4, indicating that the photogenerated electron-hole pairs in ZIF-8@Zn_2GeO_4 hybrid can be separated and transferred efficiently. That is to say, the surface electron-hole pairs recombination rate over ZIF-8@ Zn_2GeO_4 hybrid sample is the lowest, which is in good agreement with the trend in the photocatalytic activity of ZIF-8@Zn_2GeO_4 hybrid. Therefore, the photocatalytic activity of ZIF-8@Zn_2GeO_4 has been effectively improved.

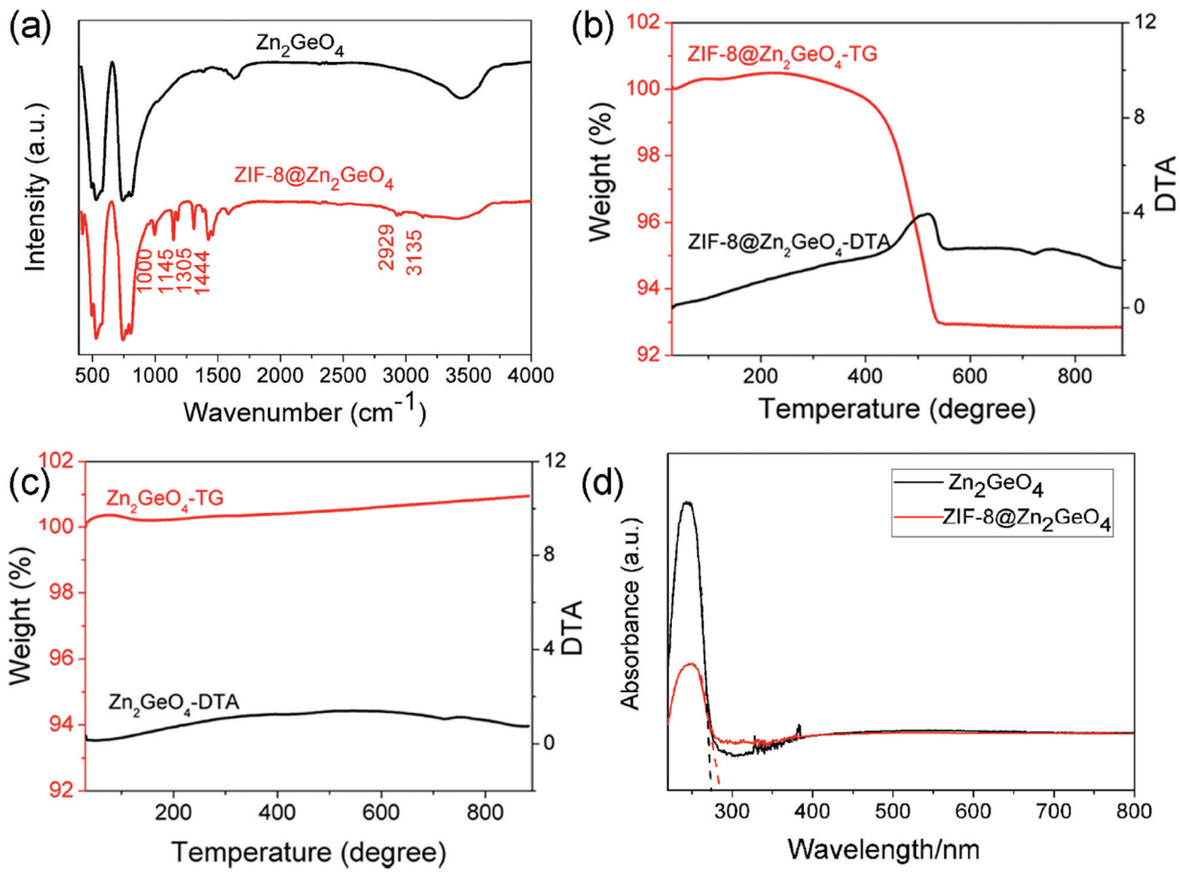

Fig. 4. (a) FTIR spectra of as-prepared Zn_2GeO_4 and ZIF-8@Zn_2GeO_4 hybrid; TG-DTA curves of (b) ZIF-8@Zn_2GeO_4 hybrids and (c) Zn_2GeO_4 nanorods; (d) UV-vis spectra of ZIF-8@Zn_2GeO_4 hybrids and Zn_2GeO_4 nanorods.

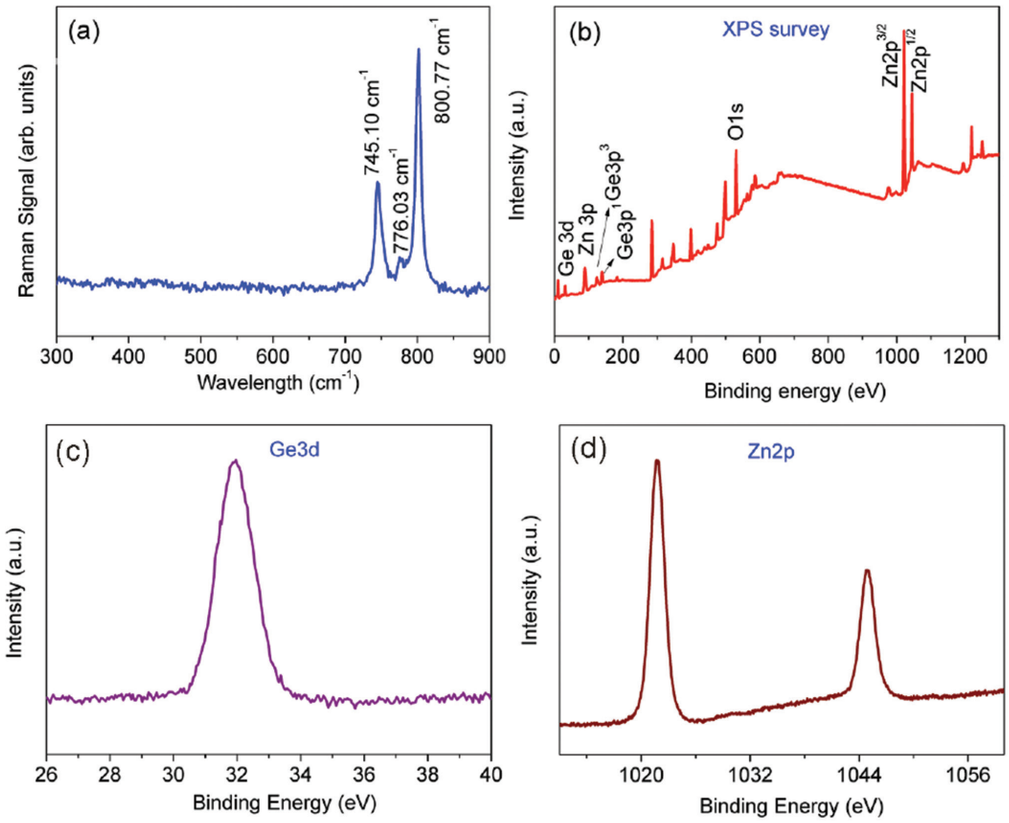

Fig. 5. The Raman spectrum of (a) ZIF-8@Zn_2GeO_4 in room temperature and XPS spectra of the prepared Zn_2GeO_4 and ZIF-8@ Zn_2GeO_4 samples: (b) survey; (c) Zn 2p; and (d) Ge 3d.

3.6. Photocatalytic activity

The photocatalytic performance of ZIF-8@Zn_2GeO_4 hybrid was investigated by evaluating the photocatalytic reduction of Cr(VI) under a 300 W Xe lamp irradiation. 0.10 g of ZIF-8@ Zn_2GeO_4 was used in 100 mL 1 × 10^{-5} mol L^{-1} Cr(VI) solution. Prior to irradiation, the suspension was stirred in the dark for 30 min to ensure that the adsorption of Cr(VI) on the surface of catalyst had reached equilibrium. As can be seen in Fig. 6, the reduction ratio of Cr(VI) is rapidly increased to nearly 100% (the blue curve in Fig. 6c) after light illumination for 90 min by using ZIF-8@Zn_2GeO_4 as photocatalyst, which is much better than that of Zn_2GeO_4 (black curve) and ZIF-8 (red curve) under identical experimental conditions. Only about 32% and 79% of Cr(VI) can be reduced by using pure Zn_2GeO_4 and ZIF-8 as photocatalyst under 180 min light irradiation, respectively.

The photocatalytic reaction kinetics of Cr(VI) photocatalytic reduction are plotted in Fig. 6d. As can be seen that the photocatalytic reduction of Cr(VI) approximately follows the pseudo-first-order kinetics, which is evidenced by the linear plot of $\ln(C_o/C)$ versus reaction time t. As results are shown in Table 1, the ZIF-8@ Zn_2GeO_4 hybrid exhibits significantly higher apparent rate constant (0.0368 min^{-1}), which is about 1.8 times and 14 times of ZIF-8 (0.0207 min^{-1}) and Zn_2GeO_4 (0.0026 min^{-1}), respectively, suggesting the enhanced photocatalytic reduction performance of Cr(VI) over ZIF-8@Zn_2GeO_4 under the same light irradiation time period. We proposed a mechanism to illustrate the enhancement of photocatalytic property of ZIF-8@Zn_2GeO_4 composite, as shown in Fig. 7. First, according to the literature reported, ZIF-8 particles exhibit positive charge in the neutral condition of pH = 7, and the negative charge of $Cr_2O_7^{2-}$ could be effectively adsorbed around the ZIF-8@Zn_2GeO_4 photocatalyst due to the electrostatic interaction [39]. Then, Zn_2GeO_4 in ZIF-8@Zn_2GeO_4 hybrids was excited, and the electrons from the excited Zn_2GeO_4 can be easily transferred to the surface of ZIF-8 and participate in the redox reaction to reduce Cr(VI) to Cr(III) through the ligand-to-metal charge transfer mechanism [40]. Zn-O-Zn chemical bonds formed between ZIF-8 and Zn_2GeO_4 suppressed the recombination of electron-hole pairs and thus slightly narrowed the band gap of ZIF-8@Zn_2GeO_4 from 4.5eV to 4.35 eV. Second, these photogenerated electrons possess a strong reduction ability (E_{CB} = –0.70 V vs. NHE at pH 7.0) and can effectively reduce the adsorbed Cr(VI) to Cr(III) ($E_{Cr(VI)/Cr(III)}$ = +0.51 V vs. NHE at pH 7.0).

The powder XRD patterns of ZIF-8@Zn_2GeO_4 sample before and after photocatalytic reaction are provided in

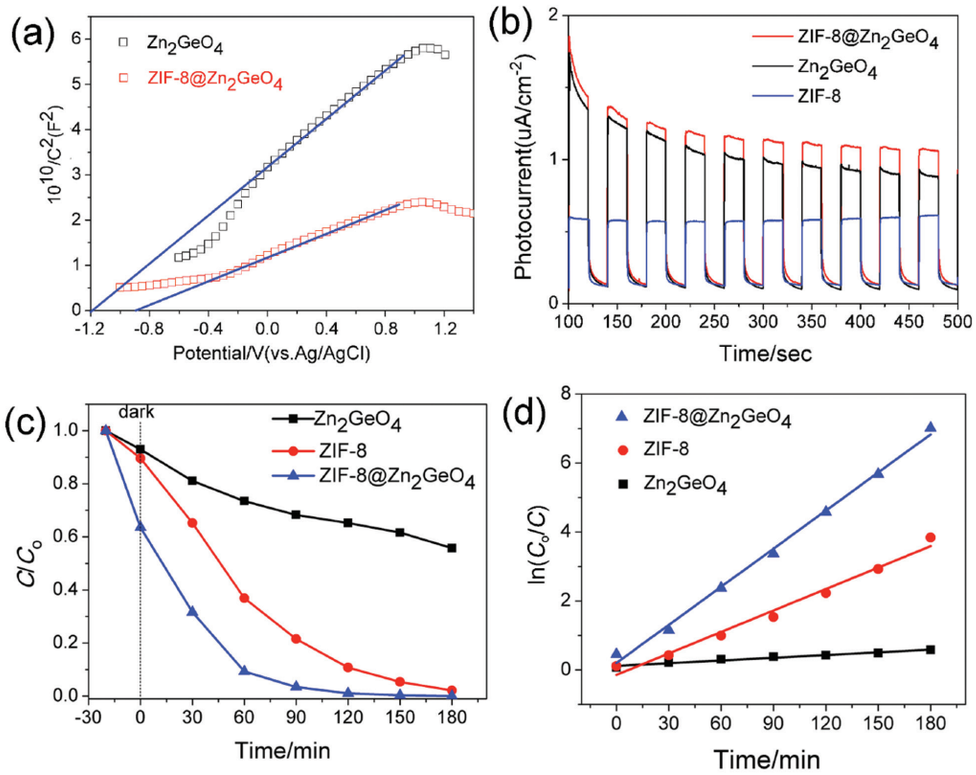

Fig. 6. (a) Mott-Schottky plots of Zn_2GeO_4 and ZIF-8@Zn_2GeO_4 in 0.2 M Na_2SO_4 aqueous solution; (b) Transient photocurrent response of ZIF-8, Zn_2GeO_4, and ZIF-8@Zn_2GeO_4 in 0.2 M Na_2SO_4 aqueous solution; (c) Photocatalytic reduction process and (d) kinetics of Cr(VI) over Zn_2GeO_4, ZIF-8, and ZIF-8@Zn_2GeO_4 hybrid.

Table 1
The pseudo-first order rate constant of Cr(VI) photocatalytic reduction over Zn_2GeO_4, ZIF-8, and ZIF-8@Zn_2GeO_4 hybrid. Reaction conditions: 100 mg of photocatalyst, 100 mL of 10^{-5} mol L^{-1} Cr(VI), pH = 7

Samples	k (min^{-1})		R
	Value	Error	
Zn_2GeO_4	0.0026	0.00019	0.9676
ZIF-8	0.0207	0.00123	0.9793
ZIF-8@ Zn_2GeO_4	0.0368	0.00108	0.9948

Fig. 8, indicating the high stability of ZIF-8@Zn_2GeO_4 sample in aqueous solution, and no other impurity phase is formed after photocatalytic reaction. Furthermore, a reusability experiment was conducted to investigate the cycling stability of ZIF-8@Zn_2GeO_4. After each recycled experiment, the used photocatalysts was recovered by filtration, washed with water and ethanol, dried in air and used for the next cycle experiments. As can be seen in Fig. 9, after 3 runs, the photocatalytic efficiency drops a little owing to the weight loss of photocatalyst in cycling experiments.

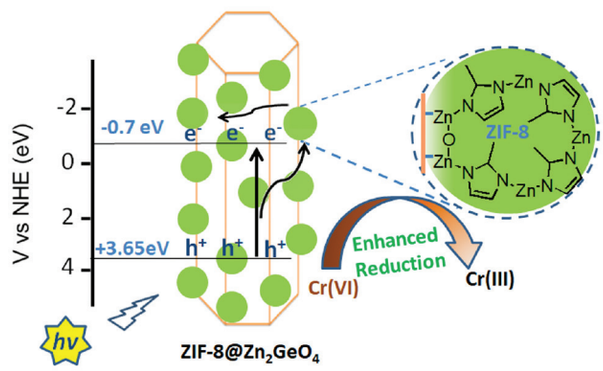

Fig. 7. A schematic diagram of the photocatalytic mechanism of the ZIF-8@Zn_2GeO_4 composite.

4. Conclusions

In summary, a binary photocatalyst ZIF-8@Zn_2GeO_4 has been successfully synthesized through chemical deposition method. About 100 mg of the obtained ZIF-8@Zn_2GeO_4 photocatalyst can reduce nearly 100% of Cr(VI) (100 mL

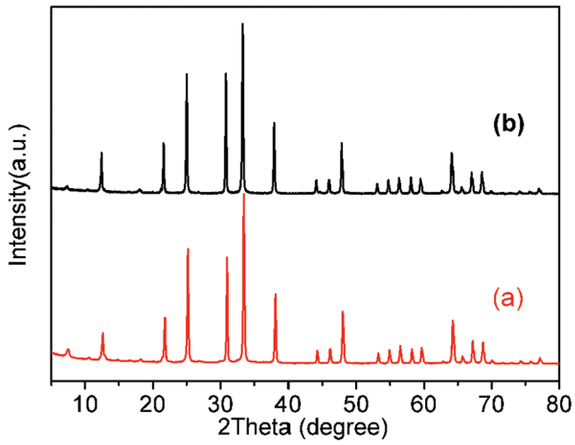

Fig. 8. The powder XRD patterns of ZIF-8@Zn_2GeO_4 sample before and after photocatalytic reaction.

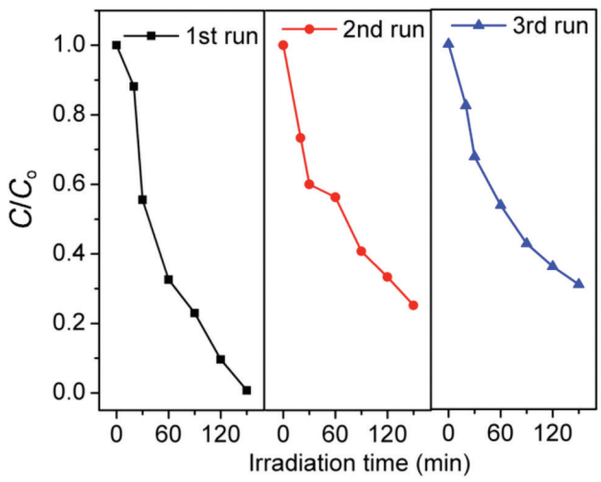

Fig. 9. Recycling experiments on ZIF-8@Zn_2GeO_4 hybrid for photocatalytic reduction of Cr(VI).

1×10^{-5} mol L^{-1}) in aqueous solution in 90 min under UV-light irradiation. The ZIF-8@Zn_2GeO_4 hybrid exhibited a higher photocatalytic activity for reduction of Cr(VI) than that of the bare ZIF-8 and Zn_2GeO_4 under the identical experimental experiments, which might be attributed to the synergetic interaction of photogenerated holes and electrons between ZIF-8 and Zn_2GeO_4. It is also expected that this kind of MOF and semiconductor combined hybrids shown here can be applied to other catalytic systems for enhanced photocatalytic efficiency.

Acknowledgments

This work was supported by the National Natural Science Foundation of China (Grant No. 21771031, 21401018) and the General Research Project of Education Department of Liaoning Province (L2014164).

References

[1] C.E. Barrera-Diaz, V. Lugo-Lugo, B. Bilyeu, A review of chemical, electrochemical and biological methods for aqueous Cr(VI) reduction, J. Hazard. Mater., 223–224 (2012) 1–12.
[2] Y. Wu, J. Zhang, Y. Tong, X. Xu, Chromium (VI) reduction in aqueous solutions by Fe_3O_4-stabilized FeO nanoparticles, J. Hazard. Mater., 172 (2009) 1640–1645.
[3] M. Haghighi, F. Rahmani, R. Dehghani, A.M. Tehrani, M.B. Miranzadeh, Photocatalytic reduction of Cr (VI) in aqueous solution over ZnO/HZSM-5 nanocomposite: Optimization of ZnO loading and process conditions, Desal. Water. Treat., 58 (2017) 168–180.
[4] M.Y. Wu, T.G. Duan, Y. Chen, Q. Wen, Y.Y. Wang, H.M. Xin, Surface modification of TiO_2 nanotube arrays with metal copper particle for high efficient photocatalytic reduction of Cr(VI), Desal. Water. Treat., 57 (2016) 10790–10801.
[5] M.R. Sammarghandi, J.K. Yang, S.M. Lee, O. Giahi, M. Shirzad Siboni, Effect of different type of organic compounds on the photocatalytic reduction of Cr (VI) in presence of ZnO nanoparticles, Desal. Water. Treat., 52 (2014) 1531–1538.
[6] X.J. Liu, T. Lv, Y. Liu, C.B. Wang, L.K. Pan, Z. Sun, TiO_2-Au composite for efficient UV photocatalytic reduction of Cr(VI), Desal. Water. Treat., 51 (2013) 3889–3995.
[7] H.Y. Huang, Y.Y. Feng, J.H. Zhou, G. Li, K.W. Dai, Visible light photocatalytic reduction of Cr(VI) on Ag_3PO_4 nanoparticles, Desal. Water. Treat., 51 (2013) 7236–7240.
[8] J.K. Yang, S.M. Lee, M. Shirzad-Siboni, Effect of different types of organic compounds on the photocatalytic reduction of Cr(VI), Environ. Technol., 33 (2012) 2027–2032.
[9] Y.C. Zhang, J. Li, M. Zhang, D.D. Dionysiou, Size-tunable hydrothermal synthesis of SnS_2 nanocrystals with high performance in visible light-driven photocatalytic reduction of aqueous Cr(VI), Environ. Sci. Technol., 45 (2011) 9324–9331.
[10] M. Pelaez, N.T. Nolan, S.C. Pillai, M.K. Seery, P. Falaras, A.G. Kontos, P.S.M. Dunlop, J.W.J. Hamilton, J.A. Byrne, K. O'Shea, M.H. Entezari, D.D. Dionysiou, A review on the visible light active titanium dioxide photocatalysts for environmental applications, Appl. Catal. B: Environ., 125 (2012) 331–349.
[11] M. Shirzad-Siboni, M. Samarghandi, J.K. Yang, S.M. Lee, Photocatalytic removal of Reactive Black-5 dye from aqueous solution by UV irradiation in aqueous TiO_2: equilibrium and kinetics study, J. Adv. Oxid. Technol., 14 (2011) 302–307.
[12] J.K. Yang, S.M. Lee, M. Farrokhi, O. Giahi, M. Shirzad Siboni, Photocatalytic removal of Cr(VI) with illuminated TiO_2, Desal. Water Treat., 46 (2012) 375–380.
[13] M. Shirzad Siboni, M.T. Samadi, J.K. Yang, S.M. Lee, Photocatalytic removal of Cr(VI) and Ni(II) by UV/TiO_2: Kinetic study, Desal. Water Treat., 40 (2012) 77–83.
[14] M. Farrokhi, J.K. Yang, S.M. Lee, M. Shirzad-Siboni, Effect of organic matter on cyanide removal by illuminated titanium dioxide or zinc oxide nanoparticles, Iran. J. Environ. Health. Sci. Eng., 11 (2013) 23.
[15] A. Jonidi-Jafari, M. Shirzad-Siboni, J.K. Yang, M. Naimi-Joubani, M. Farrokhi, Photocatalytic degradation of diazinon with illuminated ZnO–TiO_2 composite, J. Taiwan Inst. Chem. Eng., 50 (2015) 100–107.
[16] M. Naimi-Joubani, M. Shirzad-Siboni, J.K. Yang, M. Gholami, M. Farzadkia, Photocatalytic reduction of hexavalent chromium with illuminated ZnO/TiO_2 composite, J. Ind. Eng. Eng. Chem., 22 (2015) 317–323.
[17] D. Chu, J. Mo, Q. Peng, Y. Zhang, Y. Wei, Z. Zhuang, Y. Li, Enhanced photocatalytic properties of SnO_2 nanocrystals with decreased size for ppb-level acetaldehyde decomposition, Chem. Cat. Chem., 3 (2011) 371–377.
[18] J. Zhang, M. Grzelczak, Y. Hou, K. Maeda, K. Domen, X. Fu, M. Antonietti, X. Wang, Photocatalytic oxidation of water by

polymeric carbon nitride nanohybrids made of sustainable elements, Chem. Sci., 3 (2012) 443–446.
[19] M. Azita, S.A. Karimi, J.K. Yang, M. Shirzad-Siboni, Photocatalytic degradation of a textile dye by illuminated tungsten oxide nanopowder. J. Adv. Oxid. Technol., 18 (2015) 61–68.
[20] A. Mohagheghian, S.A. Karimi, J.K. Yang, M. Shirzad-Siboni, Photocatalytic degradation of diazinon by illuminated WO_3 nanopowder. Desal. Water Treat., 57 (2015) 8262–8269.
[21] Y. Xu, J. Jin, X. Li, Y. Han, H. Meng, T. Wang, X. Zhang, Simple synthesis of ZnO nanoflowers and its photocatalytic performances toward the photodegradation of metamitron, Mater. Res. Bull., 76 (2016) 235–239.
[22] M. Farrokhi, S.C. Hosseini, J.K. Yang, M. Shirzad-Siboni, Application of ZnO–Fe_3O_4 nanocomposite on the removal of azo dye from aqueous solutions: Kinetics and equilibrium studies, Water Air Soil Pollut., 225 (2014) 1–12.
[23] M.R. Samarghandi, J.K. Yang, S.M. Lee, O. Giahi, M. Shirzad-Siboni, Effect of different type of organic compounds on the photocatalytic reduction of Cr(VI) in presence of ZnO nanoparticles, Desal. Water Treat., 52 (2013) 1–8.
[24] M. Shirzad Siboni, M.T. Samadi, J.K. Yang, S.M. Lee, Photocatalytic reduction of Cr(VI) and Ni(II) in aqueous solution by synthesized nanoparticle ZnO under ultraviolet light irradiation: a kinetic study, Environ. Technol., 32 (2011) 1573–1579.
[25] M. Shirzad-Siboni, M. Farrokhi, R. Darvishi Cheshmeh Soltani, A. Khataee, S. Tajassosi, Photocatalytic reduction of hexavalent chromium over ZnO nanorods immobilized on kaolin, Ind. Eng. Chem. Res., 53 (2014) 1079–1087.
[26] M. Shirzad-Siboni, A. Khataee, B. Vahid, S. W Joo, S. Fallah, Preparation of a green photocatalyst by immobilization of synthesized ZnO nanosheets on scallop shell for degradation of an azo dye, Current Nanoscience, 10 (2014) 684–694.
[27] N.V. Kaneva, C.D. Dushkin, Tuning of the UV photocatalytic activity of ZnO using zinc ferrite(III): Powders and thin films prepared of powders, Colloids Surf. A: Physicochem. Eng. Asp., 382 (2011) 211–218.
[28] S. Yan, L. Wan, Z. Li, Z. Zou, Facile temperature-controlled synthesis of hexagonal Zn_2GeO_4 nanorods with different aspect ratios toward improved photocatalytic activity for overall water splitting and photoreduction of CO_2, Chem. Commun., 47 (2011) 5632–5634.
[29] S. Wang, X. Wang, Multifunctional metal-organic frameworks for photocatalysis, Small, 11 (2015) 3097–3112.
[30] Q. Liu, Z.X. Low, L. Li, A. Razmjou, K. Wang, J. Yao, H. Wang, ZIF-8/Zn_2GeO_4 nanorods with an enhanced CO_2 adsorption property in an aqueous medium for photocatalytic synthesis of liquid fuel, J. Mater. Chem. A., 1 (2013) 11563–11569.
[31] S. Wang, J. Lin, X. Wang, Semiconductor-redox catalysis promoted by metal-organic frameworks for CO_2 reduction, Phys. Chem. Chem. Physn., 16 (2014) 14656–14660.
[32] X. Zeng, L. Huang, C. Wang, J. Wang, J. Li, X. Luo, Sonocrystallization of ZIF-8 on electrostatic spinning TiO_2 nanofibers surface with enhanced photocatalysis property through synergistic effect, ACS Appl. Mater. Interfaces., 8 (2016) 20274–20282.
[33] X. Wang, J. Liu, S. Leong, X. Lin, J. Wei, B. Kong, Y. Xu, Z.X. Low, J. Yao, H. Wang, Rapid construction of ZnO@ZIF-8 heterostructures with size-selective photocatalysis properties, ACS Appl. Mater. Interfaces, 8 (2016) 9080–9087.
[34] M. Wang, D. Wang, Z. Li, Self-assembly of CPO-27-Mg/TiO_2 nanocomposite with enhanced performance for photocatalytic CO2 reduction, Appl. Catal. B: Environ., 183 (2016) 47–52.
[35] A. Chakraborty, S. Laha, K. Kamali, C. Narayana, M. Eswaramoorthy, T.K. Maji, In situ growth of self-assembled ZIF-8-aminoclay nanocomposites with enhanced surface area and CO_2 uptake, Inorg. Chem., 56 (2017) 9426–9435.
[36] P. Hidalgo, A. López, B. Méndez, J. Piqueras, Synthesis and optical properties of Zn_2GeO_4 microrods, Acta Mater., 104 (2016) 84–90.
[37] F. Fabregat-Santiago, G. Garcia-Belmonte, J. Bisquert, P. Bogdanoff, A. Zaban, Mott-Schottky analysis of nanoporous semiconductor electrodes in dielectric state deposited on SnO_2 (F) conducting substrates, J. Electrochem. Soc., 150 (2003) E293–E298.
[38] C. Xue, T. Zhang, S. Ding, J. Wei, G. Yang, Anchoring tailored low-index faceted BiOBr nanoplates onto TiO_2 nanorods to enhance the stability and visible-light-driven catalytic activity, ACS Appl. Mater. Interfaces, 9 (2017) 16091–16102.
[39] N.A. Khan, B.K. Jung, Z. Hasan, S.H. Jhung, Adsorption and removal of phthalic acid and diethyl phthalate from water with zeolitic imidazolate and metal-organic frameworks, J. Hazard. Mater., 282 (2015) 194–200.
[40] H.P. Jing, C.C. Wang, Y.W. Zhang, P. Wang, R. Li, Photocatalytic degradation of methylene blue in ZIF-8, RSC Adv., 4 (2014) 54454–54462.